

<https://doi.org/10.1038/s40494-025-02144-5>

# The materials of historical monuments: characterisation of the mortars of the Roman aqueduct of Zaghouan-Carthage

Check for updates

Fernanda Carvalho<sup>1,2</sup> , Maria Margarida R. A. Lima<sup>1,3</sup>, Teresa Pereira da Silva<sup>4</sup> & João Pedro Veiga<sup>1,2,5</sup>

The Zaghouan-Carthage Roman aqueduct was the largest built by the Roman Empire at the time, and its archaeological remains bear witness to the excellence of Roman construction. Its importance over the centuries makes it a unique case study for characterising the different types of mortar used. This work aims to study these materials, considering their functions, especially as structural elements or as render, to relate the chemical and mineralogical characteristics observed to both the function and historical context of the monument. Using a multi-analytical approach, the preservation of samples was prioritised whenever possible. The results indicate that mortars with a structural function have higher silicon contents than those used as render. In the case of water conduit coatings, the mortars were formulated with ground ceramics to develop hydraulic properties and ensure the waterproofing material. However, it was not possible to identify a characteristic pattern related to the historical construction periods.

Archaeological remains are material testimonies of the history, being it social of a particular region, or of the technological evolution used in the past. The Zaghouan-Carthage aqueduct is a witness to Roman construction technique and the excellent work achieved in urban structures since antiquity.

Archaeological finds show that the region of Carthage was already occupied around the 9th century BC<sup>1,2</sup>. It became a prosperous region, with trade as its main economic source. In this period, Phoenician rule, in addition to the commercial activities established with different peoples of the Mediterranean, was a source of disputes and wars. The Roman occupation began at the time of Emperor Augustus, who ruled Rome between 49 and 44 BC. The main Roman buildings in Carthage, such as the forum and other public buildings, began to be built at this time. Carthage soon became prosperous again and one of Rome's largest colonies<sup>3</sup>. Between the 1st and 2nd centuries AD, other public buildings were built, such as the amphitheatre and the circus, as well as new structures to supply the local water needs, such as fountains and cisterns. It is agreed that the visit of Emperor Hadrian to Carthage in 128 AD was the key point for his order to build the aqueduct. In the Roman context, aqueducts were essentially structures built to supply thermal baths, although the water transported could also be used for other purposes, almost always in urban environments<sup>4</sup>. It is estimated that the aqueduct was completed in 162 AD, the year in which the

construction of the Antonine Thermal Baths, supplied by the waters brought by the aqueduct, was also completed<sup>1,5</sup>.

The aqueduct of Carthage was the largest built in the Roman Empire. It had a total length of 132 km, including the main conduit and some branches<sup>3,5-12</sup>. The main conduit was just over 90 km long and drew water from a spring on the Zaghouan hill, where the *Nymphaeum* was built, with the capacity to capture between 30 and 160 l of water per second, depending on the time of year. The *Nymphaeum* had the function of accumulating water, in a kind of tank, to facilitate the collection for the conduit, in addition to being also a monument in honour of the nymphs<sup>10,12,13</sup>. A second spring, in the same region known as Aïn Ayed, with the capacity to collect between 29 and 40 l of water per second, was also used as a source of water<sup>10</sup>. Two other water collection points were connected to the main pipeline in Moghrane by a secondary pipeline southwest of Zaghouan, 33.63 km long, which drew water from the Aïn Djouggar spring, capable of collecting between 38 and 171 l of water per second, and also from the spring known as Aïn ben Saidane, capable of collecting more than 29 l per second<sup>8,10,11</sup>. Although there is no consensus on water consumption by the population of Carthage, it is estimated that the maximum flow of water transported by the aqueduct per day would be between 17,280 to 25,000 m<sup>3,5,12</sup>.

Most commonly, Roman aqueducts followed the terrain or were deliberately buried in order to avoid enemy attack, with their construction

<sup>1</sup>CENIMAT/i3N – Centro de Investigação de Materiais, NOVA FCT, 2829-516 Caparica, Portugal. <sup>2</sup>VICARTE – Vidro e Cerâmica para as Artes, NOVA FCT, 2829-516 Caparica, Portugal. <sup>3</sup>Department of Materials Science, NOVA FCT, 2829-516 Caparica, Portugal. <sup>4</sup>Mineral Resources and Geophysics Research Unit, Laboratório Nacional de Energia e Geologia (LNEG), Estrada da Portela, Bairro do Zambujal – Alfragide, Apartado 7586, 2610-999 Amadora, Portugal. <sup>5</sup>Department of Conservation and Restoration, NOVA FCT, 2829-516 Caparica, Portugal. e-mail: [fb.carvalho@campus.fct.unl.pt](mailto:fb.carvalho@campus.fct.unl.pt); [jpv@fct.unl.pt](mailto:jpv@fct.unl.pt)

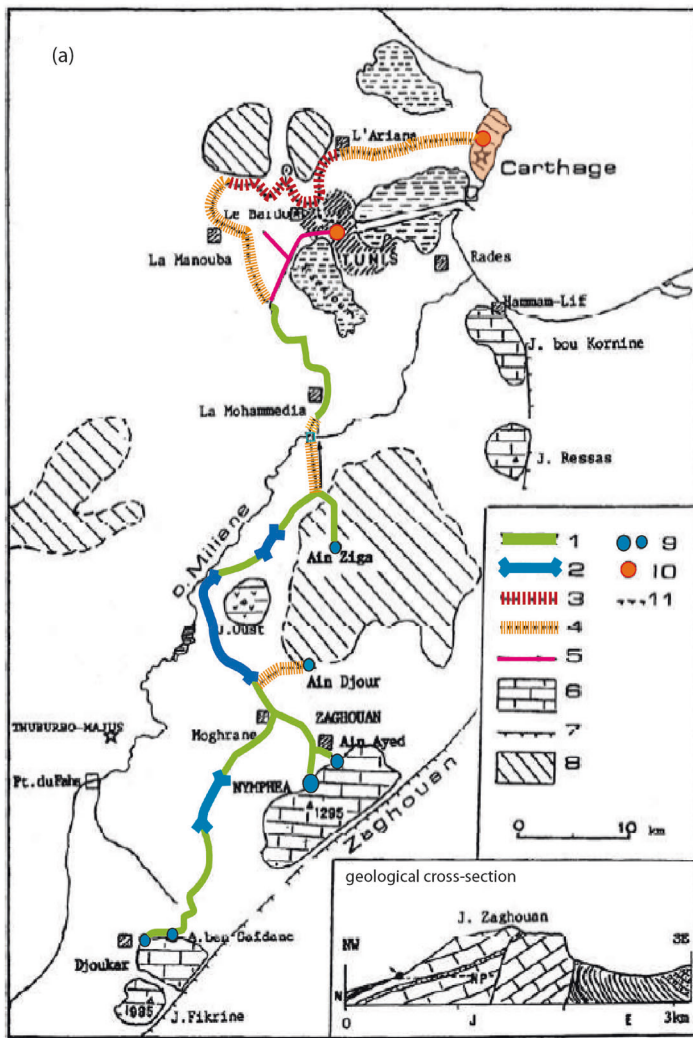


**Fig. 1 | The aqueduct of Zaghouan-Carthage.** **a** Map of the aqueduct of Carthage: 1-Main and secondary conduits, 2-Tunnel section, 3-Abandoned section, 4-section on arch, 5-Modern conduct, 6-Limestone massif, 7-Major Fault, 8-Quaternary, 9-water collection source, 10-reservoir, 11-13-century deviation. Geological cross-

section: N-Marl, J-Jurassic limestone, E-Eocene, NP-piezometric level. (Adapted from Phillippe Leveau, 10, p.5<sup>10</sup>). **b** Remnants of the water main, where you can see the construction system with its straight base and domed roof. **c** Remnants of the base of a collapsed conduit, with the mortar coating (images: J.P. Veiga).

on pillars and arches being restricted to the needs of the shortest route<sup>4,14</sup>. In Carthage it was no different. Only 17 km of the aqueduct was in aerial sections, over arcades that crossed depressions in the terrain and the valley of the Miliane River, where the arches reached 38 m in height (Fig. 1a)<sup>5,7,11,12</sup>. Most of the aqueduct was made up of a stone masonry conduit, underground, where the water flowed by gravity<sup>15,16</sup>. The Romans built the ducts with a rectangular profile, covered by a semi-circular vaulted roof, large enough for a person to stand inside, thus guaranteeing their maintenance and cleaning when necessary (Fig. 1b)<sup>3,12,14,17,18</sup>. The base and interior walls of the pipeline would be covered with lime mortar, mixed with ceramic fragments, to make the surface more regular and smoother, thus contributing to the flow of water (Fig. 1c). In addition to waterproofing the duct and preventing leaks, this coating also increased mechanical resistance. As the water occupied a maximum of 2/3 of the duct's capacity, there was no need to line the entire inside of the duct, leaving the top of the duct unlined<sup>4</sup>.

Mortars made from ground ceramic fragments were known as *Opus signinum* or popularly as “coccio-pisto” or “cocciopesto” and were systematically used as a waterproofing coating on structures intended for storing and transporting water or which were subject to the action of rain, such as cisterns, aqueducts, spas and terraces<sup>19-22</sup>. The form of preparation of this type of mortar was described by Vitruvius, in his treatise on Architecture,

although he specifically suggested the addition of pozzolan for the construction of water-resistant buildings<sup>23,24</sup>. The addition of ground ceramics, volcanic ash, and some types of silicate rocks as aggregate in a mortar imparts hydraulic properties to the material produced, even if the binder used is an area lime<sup>12,20,25,26</sup>. Hydraulic mortars have the ability to harden when submerged or in direct contact with water, improving the strength and durability of the material<sup>20,26,27</sup>.

In addition to their use as render, mortars were also used as a binding and joining element for blocks in construction. When used for this purpose, mortars contribute to improving the strength of the built structure, because in addition to contributing to load distribution, they adapt to the shapes and sizes of blocks and stones, and can even be used as filling material, making them a versatile material for different construction techniques<sup>28</sup>. In general, despite their different uses, mortars are prepared in a similar way, by mixing the binder and aggregates (usually medium-fine grain sand) with water<sup>29</sup>. In his treatise, Vitruvius describes both the methods of preparing lime, used as a binder, and indicates which sand would be best to use according to the application of the material. In the case of renders, for example, he recommends the use of river sand to prevent cracking in the mortar<sup>23,30</sup>. As with mortars used for plastering, in the case of structural mortars, the type of binder, the composition and size of the aggregates, the amount of mixing water, the pore systems, the care taken in preparation and application, and

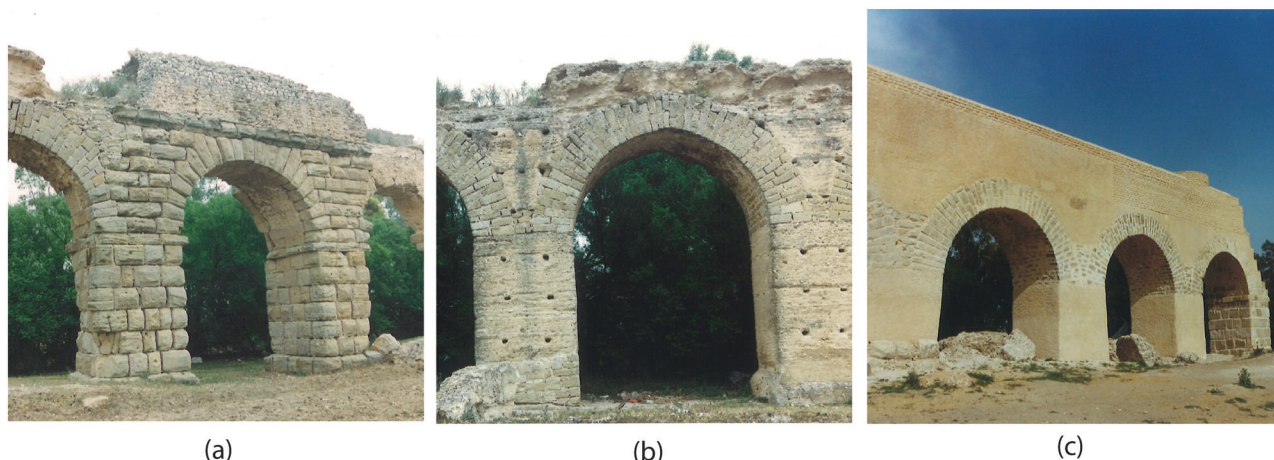


**Fig. 2 | Different building system.** **a** Roman building system opus quadratum and opus caementicium inside the pillar. **b** Medieval reconstruction of the Hafsid period. **c** Modern Reconstruction (current). (images: J.P. Veiga).

the environmental conditions will be decisive factors for the quality, durability, and efficiency of the material in performing its function<sup>28</sup>.

Different types of mortar can be found in the ruins of Carthage's aqueduct today, the result of the construction techniques involved, reconstructions and restoration work carried out over time. Regarding the construction system, in addition to the coating of the water conduits, mortars were used in the construction of the pillars that supported the conduits in the aerial sections, thus performing its structural function as a connecting element between blocks or stones, according to the construction system used<sup>29</sup>. The Roman technique used was the *opus caementicium*, in which the pillar was made up of an internal filling core, made of stones of varying sizes soaked in lime and sand mortar, covered externally by blocks of cut stones or bricks, without the use of mortar to join the blocks, although eventually there could be mortar at some points (*opus quadratum*) (Fig. 2a)<sup>3,7,12,19</sup>. Also for this case, the preference was given to mortars with pozzolanic behaviour, because they are more resistant<sup>19</sup>. As far as reconstructions are concerned, some phases are historically recognised, especially those related to the problems caused by wars. The water supply was interrupted during the Vandal occupation, between the years 439 and 533, when it was ruled by the Byzantines, and the aqueduct was repaired<sup>13,7,8,31</sup>. In 698, Carthage was taken, this time by the Arabs, and once again the aqueduct was destroyed in the aerial sections. According to Phillipe Caillat, the conquistadors themselves restored the aqueduct years later, but with different construction features<sup>31</sup>. However, the Byzantine period was marked by the abandonment of the aqueduct and the pillaging of the stones for use in other constructions, and it is not known for sure which sections of the aqueduct remained in operation<sup>5,9</sup>. It is known that new sections were built during the rule of Hafsid Sultan Abu Abdullah Mohammed I, between 1250 and 1267 (Fig. 2b), with the aim of directing water to his palace and to the supply of Tunis, since Carthage was in ruins<sup>5,9,11,13</sup>. The Spanish occupation around 1570 contributed to the dismantling and reuse of materials for new constructions<sup>7,31</sup>. It was only in the mid-seventeenth century that work was carried out to recover the aqueduct, with the aim of reestablishing its function, excluding the aerial sections that were already unrecoverable and were replaced by syphons<sup>8,18</sup>. Some parts of the ruins of the Carthage aqueduct are currently inserted in rural and urban contexts, suffering from the impact of the region's activities. Therefore, in addition to the historical interventions, various stabilisation, recovery, and reconstruction works are still being carried out on the ruins of the aqueduct (Fig. 2c), which makes this case particularly important for the study of materials used in monuments built over the years.

The aim of this study is to characterise mortar samples collected from the ruins of the Carthage aqueduct, in aerial sections, in order to identify the diversity of materials used in construction and in interventions carried out

over the years and to try to establish the relationship between the materials produced, the function of the mortars and the historical periods identified or not by archaeologists in preliminary studies<sup>7</sup>.

## Methods

For this study, 40 samples were collected at different points of the aqueduct ruins, to include a characteristic specimen of each type of construction and/or intervention identified and some unclassified samples. The mortars sampled fulfilled two basic functions in the aqueduct: structural, in this case used as filler for the Roman pillar, or used to join blocks, a construction method more representative of more modern historical periods, and render, which could have come from the main water conduit or other areas of coating from collapsed structures that were not clearly identified as conduits. From collapsed structures that were not clearly identified as conduits, being uncertain in these latter cases, the identification according to their function or historical period of manufacture/use. The periods indicated in the samples were referred to by the team of archaeologists and historians, based on in situ visual analysis and previous studies<sup>32</sup>. The proposed analytical methodology favoured the preservation of samples, whenever possible. It was necessary to prepare them in order to adapt them to the needs of the equipment used, and part of them were manually ground in an agate mortar and, another part, a cohesive fragment, was selected to be assembled in epoxy resin and polished in cross-section. The set of techniques used included<sup>20,33</sup>:

### X-ray fluorescence

Elemental chemical composition was performed on the ground samples, without separation of the binder and aggregates. X-ray fluorescence for chemical analysis was performed using an X-ray fluorescence spectrometer with a wavelength dispersive system (WDXRF) PANalytical–Axios 4.0, with a rhodium X-ray tube (20.21 keV), in conditions optimised for element quantification. The analyzing crystals of LiF220, LiF200, Ge, PE, and PX1 were used for the separation of fluorescent X-ray peaks covering all measurable range, from the element Na. Analysis was performed under He flow and spectra deconvolution using the iterative least-squares method and standardless semiquantitative analysis based on the fundamental parameter approach with the SuperQ IQ+ software package (PANalytical B.V., Almelo, The Netherlands).

### X-ray diffraction

The crystalline phases of the minerals were determined in the ground samples, using a PANalytical Xpert PRO MRD diffractometer, with X'Celerator 1D detector and Cu K $\alpha$  radiation at 45 kV and 40 mA settings, in the  $2\theta$  range of 10° to 65°, with a step of 0.02° and an acquisition time of 33 s per

step, in continuous scan mode. The identification of crystalline phases was carried out using the X'Pert High Score Plus software. The intensity of the diagnostic peaks was added by comparing the intensities obtained in the same result for the different minerals identified, in order to highlight the clear difference between the main crystalline phases identified.

### Micro-Raman

The identification of the minerals that make up the aggregates and binders was carried out in the fragments in cross-section, through the micro-Raman, in direct measurements on the observed grain. The equipment used was the Renishaw inVia Qontor micro-Raman spectrometer equipped with an air-cooled CCD detector and a HeNe laser operating at 32 mW of 633 and 532 nm laser excitation. The spectral resolution of the spectroscopic system is  $0.3 \text{ cm}^{-1}$ . The laser beam was focused with a 50 x or 100 x Olympus objective lens (N10.6 LMPLAN FL N), and the laser diameter less than 1.0  $\mu\text{m}$ . All the raw data were collected digitally with Wire 5.1 software for processing. The minerals were identified using the Spectral ID database, version 9.2, part of the GRAMS Spectroscopy Software Suite, the RRUFF online database and by comparing the results with the literature.

### Optical microscopy (OM)

All samples were observed in cross-section at the Leica DMI5000 M inverted optical microscope, with a built-in motorised platform, in reflected light. The motorised stage, microscope, and digital camera are controlled by Leica Application Suite software, version 4.12.0. The samples were observed in polarised light and dark field mode with the 5.0 and 10.0 x objectives. The study of the morphology of aggregate grains was carried out with the aid of ImageJ software, from different images obtained by OM, always at the same magnification. The apparent contours of the grains and the determination of sizes by Feret diameter were considered.

### Colorimetry

The colour study was performed on the cross-section fragments, using the CIE Lab colour space, through the parameters ( $L^*$ ,  $a^*$ ,  $b^*$ ) were determined by a portable colourimeter, TR500 Spectrophotometer Lovibond, with 4 mm aperture diameter, measurements in reflectance. Illuminant D65, observer  $10^\circ$ , data acquisition software OnShade QC v.1.7.2.520.

### Thermo-analytical techniques - simultaneous differential thermal analysis (DTA) and thermogravimetry (TG)

Thermal analysis was performed on powder samples and, as it is a micro-destructive test, it was performed on a restricted set of samples. The analyses were performed using a SETARAM 92-16.18 apparatus, incorporating a microbalance with a controlled argon gas flow (inert atmosphere). The samples were dried in an oven at  $110^\circ\text{C}$  for 2 h. About 65 mg of the milled sample were deposited in an alumina ( $\alpha\text{-Al}_2\text{O}_3$ ) crucible. The reference material was alumina powder. Therefore, the DTA-TG assays were performed in a heating temperature range from ambient to  $1100^\circ\text{C}$  at a heating rate of  $10^\circ\text{C min}^{-1}$ .

## Results

### Chemical composition (WDXRF)

The study of the elemental chemical compositions of the samples, expressed in oxides, was carried out by WDXRF, and presents a great variation in the contents of the main elements, these being the CaO (16.11–85.10%) and  $\text{SiO}_2$  (6.62–79.93%), with greater expression for the variation in CaO contents. In addition to these, the  $\text{Al}_2\text{O}_3$  (1.26–10.50%), the  $\text{Fe}_2\text{O}_3$  (0.44–5.52%) and the MgO (0.28–12.08%), among the main components of the samples studied. On the other hand,  $\text{SO}_3$  and Cl, appear in lower levels, mostly below 2% and  $\text{Na}_2\text{O}$  was detected in only three samples of the analysed set, at levels below 2.2%. Other elements identified mainly in concentrations below 0.05% or in only a few samples were added together and are presented in the 'others' column. Of the trace elements, the only one identified in all samples was strontium, generally associated with calcium, in average concentrations below 0.14% (Table 1).

Although it is not possible to identify a regular pattern in the results, considering the function of the mortars, it is possible to see that the greatest variation in these compositions occurs in those with a structural function, in which almost half of the samples show a predominance of  $\text{SiO}_2$ . In the render samples and those that were not identified, the composition also varied greatly, although CaO predominated in this case (Fig. 3).

### Mineralogical phase identification by XRD

Contrary to the variation in compositions observed in these results, the crystalline phases identified by XRD were constant for those considered to be the main ones in all the samples, with the most intense peaks corresponding to calcite and quartz. The other crystalline phases identified corresponded to the common minerals in mortars such as potassium feldspars, clays, micas, and iron oxides, although all these identified mineral phases resulted in low intensity peaks (Table 2). In one of the samples (AC\_TB8), larnite, also known as belite, was identified ( $\text{Ca}_2\text{SiO}_4$ ), which is a typical Portland cement mineral. It is noteworthy that the identification of other polymorphous phases of calcium carbonate ( $\text{CaCO}_3$ ), such as aragonite and vaterite<sup>7,21</sup>, the latter being identified in 27% of the samples analysed. The formation of vaterite may also result from the carbonation process of cementitious mortars<sup>34</sup>. During the carbonation process, calcium carbonate can precipitate in various polymorphous phases, such as calcite, aragonite and vaterite. Vaterite is thus a polymorphous form of calcium carbonate that is considered metastable; however, its formation can occur during the carbonation process and is favoured when the  $\text{Ca}^{2+}/\text{CO}_3^{2-}$  ratio is low. Furthermore, its conversion into calcite is slow in environments of high  $\text{CaCO}_3$  supersaturation<sup>35</sup>. The results obtained are consistent with other studies carried out on different mortar samples from the Carthage aqueduct, published previously<sup>7,13</sup>.

### Thermal behaviour study by TG-DTA

Still considering the overall characteristics of the material (including the binder and aggregate), a thermal study of the samples was carried out using TG-DTA analysis, where it is possible to quantify the variation in the mass of the sample due to chemical and physical changes caused in the material as the temperature rises<sup>36,37</sup>. In mortar studies, it is relevant to consider the different mass losses related to the water in the sample, as well as the losses of  $\text{CO}_2$ , characteristic of carbonate decomposition. As it is a destructive analysis, between two and three samples of each typology were selected, according to the description of the sampling. The selection criterion was based on the elemental quantification obtained by WDXRF (Table 1), to contemplate more varied elemental compositions. Table 3 shows the percentages of mass loss according to temperature, and:

- up to  $120^\circ\text{C}$  correspond to physically adsorbed water loss.
- between 120 and  $200^\circ\text{C}$  corresponds to the loss of hydration water.
- between 200 and  $600^\circ\text{C}$  correspond to the structural water loss of hydraulic compounds.
- above  $600^\circ\text{C}$  correspond to the loss of  $\text{CO}_2$  due to the decomposition of carbonates<sup>21,38–40</sup>.

The TG-DTA curves (Fig. 4) show that the endothermic peak corresponding to the decomposition of calcium carbonate occurs mostly between 830 and  $930^\circ\text{C}$ . The ARR1 sample shows the typical dolomite decomposition curve, with endothermic peaks set at  $797.77^\circ\text{C}$  and peaking at  $880.73^\circ\text{C}$ <sup>41</sup>. This result is consistent with those obtained by XRD, which also identified dolomite in this sample, along with calcite as the main phases. The DTA curves obtained from the results of the water conduit crust samples (CR13, CR28I and CR20) show inflection points at the endothermic peak of calcite decomposition, which indicates that these samples may have different types of binders. This type of result is more common in materials such as cements or hydraulic mortars<sup>41</sup>.

By thermal analysis, it is possible to calculate the hydraulicity index of a mortar, through the ratio between the loss of  $\text{CO}_2$  due to carbonate decomposition and structural water loss, occurring between 200 and  $600^\circ\text{C}$  (Table 3). The ability of a mortar to set in air (aerial mortar) or in water (hydraulic mortars)<sup>42</sup> is directly related to the minerals formed during the

**Table 1 | Elemental composition obtained by WDXRF for mortar samples from the Carthage aqueduct**

Samples	Function	Period	CaO	SiO <sub>2</sub>	Al <sub>2</sub> O <sub>3</sub>	Fe <sub>2</sub> O <sub>3</sub>	K <sub>2</sub> O	MgO	SO <sub>3</sub>	Na <sub>2</sub> O	Cl	Others
AG9	S	U	46.87	39.68	6.20	3.42	1.22	1.13	0.45	-	0.39	0.65
HAF31	S	U	78.16	13.49	2.81	2.26	0.69	0.66	0.44	-	1.10	0.39
AG29	S	U	85.10	6.62	1.91	1.27	0.36	1.33	2.54	-	0.54	0.33
HAF42	S	Me	54.19	28.10	7.41	4.37	1.89	1.84	0.31	-	1.04	0.70
AG14	S	Ro	16.11	79.93	1.82	0.68	0.28	0.28	0.62	-	0.12	0.17
AJ21	S	Ro	44.1	51.1	1.26	0.44	0.22	1.12	1.06	-	0.33	0.37
AJ22	S	Ro	33.61	54.32	2.74	1.08	0.91	1.76	1.59	1,31	2.20	0.48
AJ24	S	Ro	29.79	64.98	1.39	0.78	0.38	1.00	1.12	-	0.31	0.25
BR3	S	Ro	63.25	31.12	2.81	1.41	0.21	0.75	0.22	-	0.03	0.20
HAF34	S	Me	78.38	14.20	3.18	1.89	0.72	0.89	0.24	-	0.05	0.45
AG10	S	Ro	40.68	48.18	3.71	1.57	0.35	0.77	3.81	-	0.63	0.31
CR4b	R	Ro	60.53	27.79	4.86	3.27	0.42	1.09	0.95	-	0.48	0.61
CR12	R	Ro	47.09	33.19	8.39	5.24	0.89	1.78	0.78	-	1.85	0.80
CR20	R	Ro	31.49	46.02	10.5	3.73	3.84	0.92	0.71	1,26	0.79	0.74
AG5	R	U	51.76	40.81	3.48	1.59	0.67	0.73	0.43	-	0.24	0.29
CR13	R	Me	54.86	32.92	5.29	2.59	0.33	1.50	0.87	-	0.90	0.75
HAF38	R	Me	59.67	25.99	6.44	3.89	0.67	1.51	0.54	-	0.68	0.62
CR11	R	U	56.15	25.61	7.68	5.02	1.08	1.67	0.33	-	0.99	1.46
CR17	R	U	59.79	25.5	7.15	3.56	1.42	1.39	0.32	-	0.26	0.62
CR18a	R	U	44.90	32.90	10.10	5.52	1.52	2.13	0.29	0,94	0.66	1.05
CR23	R	U	36.17	39.17	9.95	5.40	1.12	6.83	0.23	-	0.12	1.00
CR27	R	U	56.00	30.04	5.53	3.83	0.14	1.56	0.63	-	1.08	1.19
CR28a	R	U	39.93	33.24	7,79	3.58	1.64	12.08	0.51	-	0.36	0.86
TB33	R	Mo	48.02	42.12	4.64	1.59	0.86	0.85	0.55	-	1.11	0.27
HAF26b	R	Mo	54.66	35.94	4.80	1.85	0.59	0.73	0.11	-	0.03	1.28
ARR32	R	Mo	74.19	16.00	3.01	2.45	0.30	1.05	0.82	-	1.55	0.63
CR19	R	Mo	54.70	30.90	6.38	4.18	0.58	1.80	0.69	-	-	0.77
ARR1	U	Mo	50.88	35.25	3.06	3.84	0.65	5.53	0.35	-	0.21	0.23
ARR6	U	Mo	63.39	27.17	3.92	2.01	0.70	1.01	0.52	-	0.12	1.16
TB8	U	Mo	63.64	24.59	4.87	4.16	0.79	1.02	0.58	-	0.05	0.30
TB25	U	Mo	84.10	9.32	2.85	1.53	0.49	1.18	0.17	-	0.02	0.34
HAF7	U	Me	58.67	26.38	5.22	4.83	0.47	1.00	1.38	-	1.36	0.69
AG16	U	Me	72.33	17.78	4.12	2.40	0.76	1.13	0.19	-	0.71	0.59
HAF35	U	Me	57.62	28.51	6.52	3.67	0.40	1.39	0.82	-	0.40	0.68
HAF37	U	Me	59.00	26.5	7.02	4.39	0.76	1.25	0.31	-	0.11	0.66
BR36	U	Ro	44.87	44.67	5.70	2.54	0.80	0.87	0.13	-	0.04	0.39
AG2	U	U	41.03	47.03	6.20	2.70	1.70	0.60	0.11	-	0.08	0.54
AG39c	U	U	60.68	27.19	5.16	2.84	0.97	0.99	0.84	-	0.41	0.92
AG40a	U	U	71.65	18.49	4.79	2.2	0.82	0.95	0.31	-	0.36	0.44
AG41	U	U	54.19	28.10	7.41	4.37	1.89	1.84	0.31	-	1.20	0.70

S structural mortar, R rendering mortar, Me medieval, Mo modern, Ro Roman, U undefined. (-) not detected; Others = NiO, ZnO, Rb<sub>2</sub>O, SrO, ZrO<sub>2</sub>, As<sub>2</sub>O<sub>3</sub>, BaO, Nb<sub>2</sub>O<sub>5</sub>.

hardening reaction, which in turn will have an impact on the percentage of structural CO<sub>2</sub> and H<sub>2</sub>O loss measured during thermal analysis. The result obtained with the CO<sub>2</sub>/H<sub>2</sub>O ratio is inversely proportional to the hydraulic character, i.e. the higher the resultant value, the lower the hydraulic character. Therefore, ratios above 10 correspond to mortars considered aerial, between 5 and 10 are considered mortars with a medium to low hydraulic character, between 3 and 5 are considered hydraulic mortars and below 3 are considered pozzolanic or mortars with a strong hydraulic character<sup>21,39,43–45</sup>. It is important to note that mortars containing calcite aggregates will have an influence on this result, since the decomposition of these minerals is not distinguishable from the decomposition of the binder. Still, it is possible to

consider these ratios as a good indicator of the hydraulic character of the mortars. The results obtained indicate that the mortars considered modern or used in more recent restoration interventions, being TB25, ARR1 and ARR6, are those that presented the highest hydraulicity indexes, corresponding to aerial mortars. The second sample of this typology (TB8), which is also considered a more modern material, has a hydraulicity index compatible with a mortar with some hydraulic character. This result is consistent with those obtained in XRD analyses, since the crystalline phase of belite, a typical cement mineral, was identified in this sample. The fact that the hydraulicity index of this sample specifically does not correspond to the characteristic index of pozzolans, may indicate that this material is the result

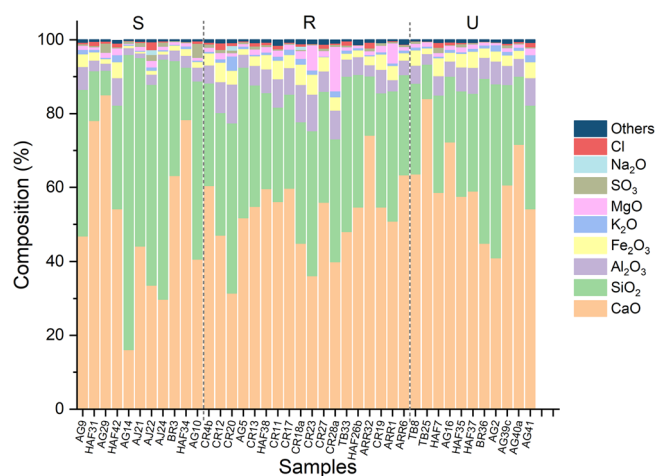


**Fig. 3** | Elemental composition of the mortar samples from the Carthage Aqueduct, depending on the function of the material, where 'S' is the samples with structural function, 'R' is the rendering mortar and 'U' is the undefined mortar.

of a mixture of overhead binders with cement, for example. All samples collected from the water conduit (CR13, CR20 and CR28I) showed indices compatible with pozzolans or strongly hydraulic mortars, as expected due to the function they performed in the monument. The samples identified as typical of the Hafsid period (HAF26b and HAF7) or medieval also showed hydraulicity indices compatible with hydraulic mortars, as well as the other samples analysed.

#### Aggregates mineralogical identification by micro-Raman

The specific aspects related to the aggregates, and the binder were studied in the mortar fragments assembled in resin and polished in cross-section. By micro-Raman, the identification of minerals is done through direct analysis on the observed grain<sup>46,47</sup>. In this way, it is also possible to identify minerals that are in smaller proportions, the result of which is not detectable or evident by other techniques. Figure 5 shows the main results obtained in this study. As expected, quartz was identified in all samples ( $\text{SiO}_2$ ) as the main component of sands and calcite ( $\text{CaCO}_3$ ) as the main mineral corresponding to the binder zone (Fig. 5a). The identification of quartz as the main component mineral of the aggregates was expected, since sand is an abundant component, historically indicated and used for the preparation of lime mortars. Quartz is known to be chemically inert. By mixing it with the binder, it plays an important role in containing the retention that occurs in the binder during the hardening phase of the mortar, improving its mechanical strength and the appearance of cracks<sup>23,29,48,49</sup>. Calcite has also been identified as an aggregate in some samples. The main difference between the results obtained was related to the intensity of the peaks, which were always lower in the case of calcites identified in the binder zone. It is important to note that the size of the grain and the crystal structure of the mineral have an influence on the intensity of the Raman bands, as well as the characteristics of the grain surface and the laser used<sup>50,51</sup>. Aragonite, one of the polymorphs of calcium carbonate ( $\text{CaCO}_3$ ), was identified in at least one sample collected from the water conduit, in which this mineral had not been identified by XRD. Figure 5a shows the differences in the positioning of the vibration bands relative to the two polymorphs identified, and the symmetrical distension band of the carbonate group ( $\text{CO}_3$ )—1087 and 1085  $\text{cm}^{-1}$ , is slightly deviated in the aragonite, while the in-plane bending and lattice vibration bands, centred at 705 and at 206  $\text{cm}^{-1}$ , respectively, they present more evident deviations when compared to the analogous vibration bands observed in the calcite result<sup>52</sup>. In addition to these minerals, potassium feldspars and iron oxides, such as haematite and magnetite, were frequently identified (Fig. 5a)<sup>53–55</sup>. Carbonaceous particles (Fig. 5b) were identified in some results. In fact, some samples showed charcoal-like fragments when observed under light microscopy. Charcoal and ash can be

incorporated into the mortar as aggregates or as additives to change the final colour of the prepared material, making it darker; however, these are relatively common impurities resulting from furnaces and calcination processes<sup>56</sup>. Identification of typical cement minerals, such as alite ( $3\text{CaO}\cdot\text{SiO}_2$  or  $\text{C}_3\text{S}$ ), larnite (belite) ( $2\text{CaO}\cdot\text{SiO}_2$  or  $\text{C}_2\text{S}$ ), and ferrite ( $4\text{CaO}\cdot\text{Al}_2\text{O}_3\cdot\text{Fe}_2\text{O}_3$  or  $\text{C}_4\text{AF}$ )<sup>52</sup> it was more common in the results of samples referenced as Hafsid and also in samples of the conduits, although they were identified in a few samples. These minerals are the result of the calcination process of the raw materials used to manufacture cement, such as limestone, clays, sands, and iron minerals, all of which are calcined at high temperatures (above 1400 °C). Finding them in a mortar means that the material was certainly produced after the 19th century, since the cement resulting from this calcination process was only developed in this period or that it is part of the set of samples corresponding to the most recent interventions. Two results were isolated cases, being talc identified in a coating sample referred to as Hafsid (AC\_HAF26) and gypsum, also identified in a coating sample collected in the water conduit (AC\_CR23), which was also identified in the XRD result of this sample.

#### Other characteristics observed by OM and colorimetry

The study of the colour and the main characteristics observed in relation to the size, abundance and distribution of the grains is presented in Table 4. Considering the total set of samples, it was not possible to determine an evident pattern, neither by observing the samples according to the function performed, nor by considering them according to the reference indicated by the team at the time of sampling. Even so, it is possible to see that the materials used with structural function tended to be darker and those used in the coatings tended to be lighter, although this is not true for all the samples observed. Figure 6 illustrates some examples of the variation of the samples observed in OM, according to the function. Regarding the variation of grain size, it is also possible to see that the duct coating mortars are those that have the smallest grains, when compared to samples with structural functions, although it is also not possible to determine a standard. In this case, it is important to mention that the coating of the pipeline was made in different layers, in which the size of the grains was greater in the innermost layers, applied next to the substrate. The shape of the grains also varies between samples; however, in general, there is a predominance of sub-angular, sub-rounded and rounded grains<sup>57</sup>, without a defined pattern observed. In general, these samples have well-graded aggregates and a mostly heterogeneous distribution. The samples with coating function were those that showed fragments of ground ceramic (*cocciopesto*), especially in the samples from the water conduits. Samples with a coating function also showed charcoal-like fragments (see ARR32, Fig. 6). This type of mortar also presented more cohesive fragments, i.e. without disintegration between binder and aggregate, with less porosity or apparent cracks. On the other hand, the mortars used with structural function showed apparent porosity and cracks of both a mechanical nature and those possibly caused by shrinkage in all the samples observed. In these cases, no fragments of pottery or charcoal were observed. Bioclasts were observed in some samples, the most frequent being those with an elongated structure, greyish-white in colour, similar to the fragment observed in the upper right corner of the image referring to the HAF42 sample, shown in Fig. 6.

#### Discussion

As previously mentioned, the addition of ground ceramics to lime mortars was intended to impart hydraulic properties that, in addition to resulting in a mechanically stronger material, contributed above all to the waterproofing of the area where it was applied. In the case of water conduits, this property was essential to preserve them from possible leaks. These results prove the care in the adequacy between raw materials and preparation of the material, depending on its application and use. In addition, the fact that the most cohesive fragments were also observed only in the cases of samples used as coating may be related to the application technique of this type of mortar. To ensure the quality of the coating, it is important to pay attention to the amount of water added to the mix, the mixing of all the components and the

**Table 2 | Crystalline phases identified by XRD**

Samples	Qz	Cal	Vtr	Arg	Dol	Ab	Gp	Hem	Bt	Fsp	HI	Ms	Px	Lrn
AG9	++++	+++	-	-	-	-	-	-	-	-	-	-	-	-
HAF31	++	++++	-	-	-	+	-	-	-	-	-	-	-	-
AG29	++	++++	-	-	-	-	+	-	-	-	-	-	-	-
HAF42	+++	++++	-	+	-	-	-	+	-	-	-	-	-	-
AG14	++++	++	-	-	-	-	-	+	-	-	-	-	-	-
AJ21	++++	++	-	-	-	-	-	-	-	-	-	-	-	-
AJ22	++++	++	-	-	-	-	-	-	-	+	+	-	-	-
AJ24	++++	++	-	-	-	-	-	-	-	-	-	-	-	-
BR3	+++	++++	-	-	-	-	-	+	-	-	-	-	-	-
HAF34	++	++++	-	-	-	-	-	-	-	-	-	-	-	-
AG10	++++	+++	-	-	-	-	+	-	-	-	-	-	-	-
CR4b	++	++++	+	-	-	-	-	-	-	-	-	+	-	-
CR12	++	++++	-	-	-	-	-	++	-	-	-	+	-	-
CR20	+++	++++	-	-	-	-	-	-	-	++	-	-	-	-
AG5	++++	+++	-	-	-	-	-	-	-	-	-	-	-	-
CR13	++++	+++	+	-	-	-	-	-	-	-	-	-	-	-
HAF38	+++	++++	+	-	-	-	-	-	-	-	-	-	-	-
CR11	++	++++	-	-	-	-	-	+	+	-	-	-	-	-
CR17	++	++++	-	-	-	-	-	-	+	-	-	-	-	-
CR18a	+++	++++	-	-	-	-	-	-	-	-	-	-	+	-
CR23	++++	+++	-	-	-	-	+	+	+	+	-	-	-	-
CR27	++	++++	+	-	-	-	-	-	-	+	-	-	-	-
CR28a	+++	++++	+	+	-	+	+	-	-	+	-	-	-	-
TB33	++++	+++	+	-	-	-	-	-	-	+	-	-	-	-
HAF26b	+++	++++	-	-	-	-	-	-	-	-	-	-	-	-
ARR32	++	++++	-	-	-	-	-	-	-	-	-	-	-	-
CR19	++	++++	+	-	-	-	-	-	-	-	-	-	-	-
ARR1	+++	++++	+	-	++	-	-	-	-	-	-	-	-	-
ARR6	++	++++	-	-	-	-	-	+	-	-	-	+	-	-
TB8	+++	++++	-	-	-	-	-	-	-	-	-	-	-	++
TB25	++	++++	-	-	-	-	-	-	-	-	-	-	-	-
HAF7	++	++++	-	-	-	-	-	+	-	-	-	-	-	-
AG16	++	++++	-	-	-	-	-	-	-	-	-	-	-	-
HAF35	+++	++++	+	-	-	-	-	-	-	+	-	-	-	-
HAF37	++	++++	+	-	-	-	-	-	-	+	-	-	-	-
BR36	+++	++++	+	-	-	-	-	-	-	-	-	-	-	-
AG2	+++	++++	-	-	-	-	-	-	-	++	-	-	-	-
AG39c	++	++++	-	-	-	-	-	-	-	-	-	-	-	-
AG40a	+	++++	-	-	-	-	-	-	-	-	-	-	-	-
AG41	++	++++	-	-	-	-	-	-	-	+	-	-	-	-

Main diagnostic peak intensity: (++++) very intense; (+++) intense; (++) weak; (+) very weak; (-) not detected.

Quartz (Qz) (SiO<sub>2</sub>); Calcite (Cal) (CaCO<sub>3</sub>); Vaterite (Vtr) (CaCO<sub>3</sub>); Aragonite (Arg) (CaCO<sub>3</sub>); Dolomite (Dol) (CaMg(CO<sub>3</sub>)<sub>2</sub>); Albite (Ab) (NaAlSi<sub>3</sub>O<sub>8</sub>); Gypsum (Gp) (CaSO<sub>4</sub>·2H<sub>2</sub>O); Haematite (Hem) (Fe<sub>2</sub>O<sub>3</sub>); Biotite (Bt) (K(Fe<sup>2+</sup>/Mg)<sub>2</sub>(Al/Fe<sup>3+</sup>/Mg/Ti)(Si/Al/Fe<sub>2</sub>Si<sub>2</sub>O<sub>10</sub>(OH/F)<sub>2</sub>); K-Feldspar (Fsp) (K(AlSi<sub>3</sub>O<sub>8</sub>)); Halite (HI) (NaCl); Muscovite (Ms) (KAl<sub>2</sub>(AlSi<sub>3</sub>O<sub>10</sub>(OH)<sub>2</sub>); Pyroxene (Px) (ADSi<sub>2</sub>O<sub>6</sub>); Lamite (Lrn) (Ca<sub>2</sub>SiO<sub>4</sub>).

compression of the mortar against the substrate. All these factors will have an impact on the contraction of the mortar during setting and also on the resistance of the material to cracking<sup>44,48</sup>. The presence of pores and cracks in render mortars may also be related to the size of the aggregate grains used, and finer sands tend to require a greater volume of water at the time of kneading, which also implies a greater volume of evaporated water, which will contribute to a larger pore system, especially on the surface. In addition, lime binders also tend to require a higher volume of kneading water, due to the specific surface of the lime, which will impact the shrinkage of the

material during the mortar hardening process<sup>57-59</sup>. Therefore, it is important to compress the coating at the time of application in order to minimise the formation of cracks and larger pores on the surface.

Mortars with a structural function also consist of mixtures of lime-based binders, sand and water. The results of this study indicated that mortars used for structural purposes generally had a similar average particle size to that observed for render mortars; however, cracks and porosity were observed more frequently in the structural samples. This fact may be directly related to the way structural mortars are applied, since, in this case, it does

**Table 3 | Percentages of mass losses in relation to the temperature ranges of interest, calculated using the results obtained by TG-DTA**

Samples	Mass loss according to temperature (%)				Total mass loss (%)	CO <sub>2</sub> /H <sub>2</sub> O
	<120 °C	120–200 °C	200–600 °C	>600 °C		
AC_AG5	1.87	1.67	5.54	17.20	26.28	3.11
AC_AG10	1.82	1.64	3.67	14.45	21.58	3.94
AC_TB25	0.85	0.39	1.51	37.13	39.88	24.63
AC_TB8	0.69	0.77	2.47	17.83	21.76	7.21
AC_HAF26B	2.18	2.18	4.11	19.79	28.26	4.81
AC_HAF7	2.37	1.87	7.30	21.13	32.67	2.90
AC_CR28I	3.43	2.61	6.70	16.23	28.97	2.42
AC_CR20	2.32	2.65	5.12	11.67	21.77	2.28
AC_CR13	2.05	1.68	6.05	19.65	29.43	3.25
AC_BR3	1.32	1.17	3.50	23.12	29.11	6.60
AC_ARR6	0.94	0.62	2.60	28.89	33.05	11.11
AC_ARR1	0.75	0.48	1.96	25.75	28.94	13.11

The ratio CO<sub>2</sub>/H<sub>2</sub>O was calculated to determine the hydraulicity index of the analysed samples.

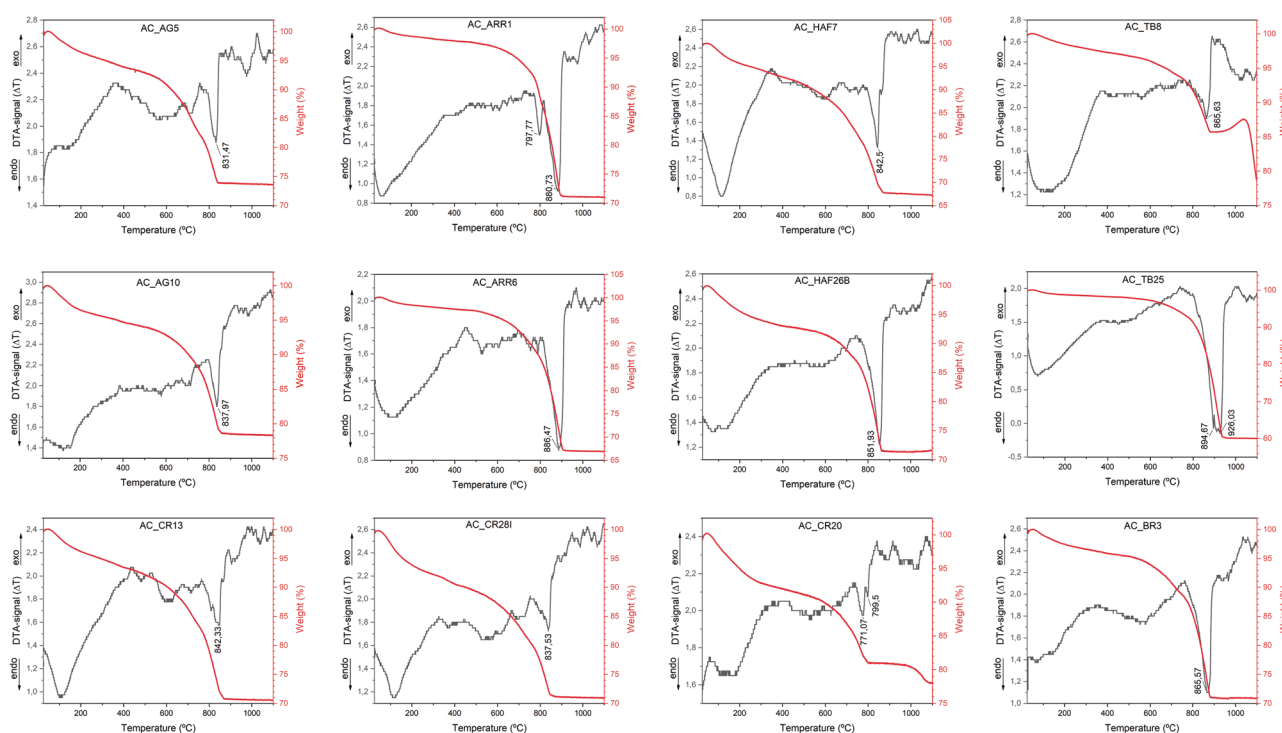


**Fig. 4 | TG-DTA curves of the samples analysed.** All the results show the TG curve defined for the transformation of CO<sub>2</sub>, but with more subtle inflections in samples AG5, HAF9, CR13, CR28I and BR3. Only sample CR20 showed a clear inflection corresponding to the decompositions that took place between 770 and 800 °C.

not involve the same type of compression as that observed in the application of coatings, which may favour the formation of cracks resulting from both water evaporation during setting and those of a mechanical nature.

Considering the set of samples from collapsed areas of the aqueduct, whose function was not clearly identified, considering the characteristics observed in OM and the other results presented in this study, it is possible to suggest that most of this set corresponds to the mortars used as coating.

The importance and extension of the Carthage aqueduct make this monument a unique opportunity to study the variations that characterise the mortars used for different functions. It is important to note that these are composite materials, resulting from the mixture of the binder with sand and water, regardless of the period in which this material was prepared. Still,

ensuring the functional performance of the material is a priority, so it is expected that it will be possible to identify trends regarding the function of the mortars. When used with a structural function, either as a block junction or as a pillar filler, in general, they presented higher silicon contents, with quartz being identified as the main crystalline phase. This result is consistent with mortars rich in siliceous sand, which guarantee volumetric stability and confer chemical and mechanical resistance to the mortar. These characteristics are important for the material to perform its function. Naturally, other factors such as the shape and size of the grains will also play an important role in the performance of the mortars; however, when considering these aspects of the aggregates, it was not possible to identify a typical pattern depending on the function of the mortar. In the case of

**Fig. 5 | Main results obtained by micro-Raman analyses.** **a** More frequent results, with quartz and calcite being observed in all samples. **b** Less frequent results or minerals identified only once from the sample set.

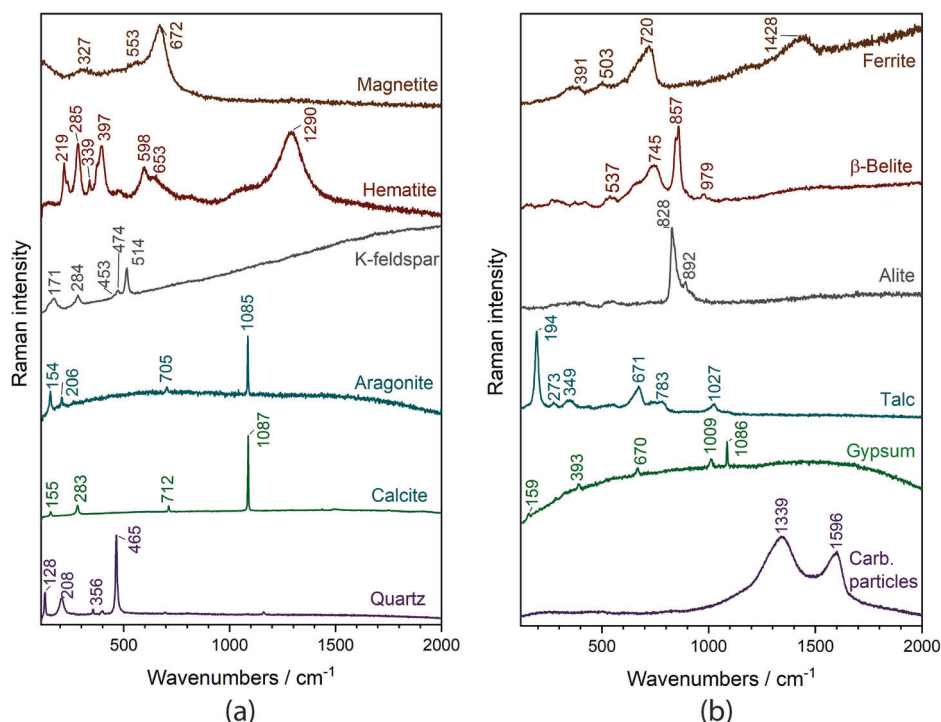




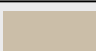
**Table 4 | Summary of the main characteristics observed by OM and colorimetry, according to the function of the mortars**

Samples	Function	Colours	L*, a*, b*	Size variation (µm)	Average size (µm)	Aggregate abundance	Distribution	Other observations
AG9	S		76.85, 2.50, 17.17	66.07 – 244.46	133.78	++++	heterogeneous	Pores, cracks
HAF31	S		59.80, 3.21, 14.93	82.91 – 776.58	229.66	++	heterogeneous	Pores, lumps
AG29	S		56.65, 13.74, 26.34	54.57 – 221.53	104.74	++	heterogeneous	Pores, cracks
HAF42	S		52.52, 4.70, 15.27	114.00 – 954.62	360.37	++++	heterogeneous	Pores, Bioclast
AG14	S		56.50, 4.26, 15.13	79.79 – 995.16	280.45	++++	homogeneous	Pores
AJ21	S		65.22, 5.91, 19.46	123.59 – 745.89	327.08	++++	homogeneous	Pores
AJ22	S		41.94, 4.99, 14.89	126.77 – 1610.58	268.24	++++	heterogeneous	Pores, cracks
AJ24	S		67.06, 5.56, 19.92	73.16 – 1176.08	251.29	++++	homogeneous	Pores, cracks
BR3	S		70.41, 5.30, 17.20	69.41 – 718.18	299.83	+++	heterogeneous	Pores, cracks
HAF34	S		48.54, 7.75, 15.03	55.80 – 906.96	261.63	++	heterogeneous	Pores, cracks
AG10	S		66.88, 6.15, 17.96	64.23 – 1687.41	268.24	+++	heterogeneous	Cracks
CR4b	R		77.13, 2.55, 12.49	52.96 – 831.74	229.50	++++	heterogeneous	Pores, cracks Ceramic, lumps
CR12	R		61.84, 2.23, 12.45	62.69 – 478.84	159.19	++++	heterogeneous	cracks, ceramics

**Table 4 (continued) | Summary of the main characteristics observed by OM and colorimetry, according to the function of the mortars**

Samples	Function	Colours	L*, a*, b*	Size variation (µm)	Average size (µm)	Aggregate abundance	Distribution	Other observations
CR20	R		75.43, 2.36, 13.30	53.38 – 1490.58	222.43	++++	heterogeneous	cracks. Ceramics, Bioclast, lumps
AG5	R		88.28, 2.04, 7.87	69.16 – 719.28	236.32	++++	homogeneous	Cohesive Lumps
CR13	R		48.17, 0.80, 7.32	132.01 – 1841.03	450.21	+++	heterogeneous	Cracks. Coal, ceramics
HAF38	R		59.02, 2.80, 12.60	51.04 – 1150.51	219.86	+++	heterogeneous	Cracks Coal, ceramics.
CR11	R		58.15, 6.55, 13.82	96.01 – 1220.87	319.50	++++	heterogeneous	Cracks. Ceramics
CR17	R		61.85, 6.96, 15.62	41.83 – 799.83	196.12	++++	homogeneous	Pores, cracks Ceramics
CR18a	R		63.78, 6.11, 15.49	58.56 – 1779.73	230.30	++++	homogeneous	Cohesive Ceramics
CR23	R		72.75, 6.87, 12.59	56.50 – 767.81	185.67	++++	homogeneous	Pores, cracks Ceramics, lumps
CR27	R		77.64, 2.68, 12.26	51.88 – 1363.03	297.00	++++	heterogeneous	Pores, cracks Ceramics, Bioclast
CR28a	R		76.35, 4.95, 11,71	42.69 – 1315.70	174.85	++++	heterogeneous	Pores, cracks Ceram., lumps
TB33	R		86.16, 2.32, 10.10	49.07 – 1288.92	287.74	+++	heterogeneous	Pores, cracks
HAF26b	R		87.50, 2.42, 10.55	49.56 – 942.09	221.08	++++	heterogeneous	cracks, lumps
ARR32	R		72.37, 0.92, 9,43	67.10 – 879.78	274.54	++	heterogeneous	Pores, cracks. Coal
CR19	R		60.91, 5.57, 18.15	66.78 – 820.85	228.85	+++	heterogeneous	Cohesive
ARR1	U		46.65, 6.71, 17.32	97.67 – 1513.25	408.41	+++	heterogeneous	Pores Ceramics, Bioclast
ARR6	U		48.64, 3.28, 11.18	57.15 – 1440.69	332.54	+++	heterogeneous	Pores, cracks Ceramics, Bioclast
TB8	U		49.40, 0.50, 7.07	68.88 – 934,06	233.75	++++	homogeneous	Pores Coal
TB25	U		56.27, 11.66, 20.88	51.95 – 727.76	221.50	++	heterogeneous	Pores, cracks. Ceramics, lumps
HAF7	U		56.84, 4.22, 15.10	124.30 – 1851.72	372.69	+++	heterogeneous	Pores, cracks
AG16	U		60.22, 10.53, 21.52	58.90 – 799.59	214.55	++	heterogeneous	Poros, cracks. Ceramics, lumps
HAF35	U		68.15, 12.32, 23.48	66.19 – 822.35	189.25	+++	heterogeneous	Cracks Ceramics, coal
HAF37	U		65.36, 13.72, 25.83	53.09 – 978.76	227.29	+++	heterogeneous	Ceramics, Bioclast
BR36	U		90.55, 1.02, 6.84	59.72 – 998.11	221.11	+++	heterogeneous	Pores, cracks
AG2	U		87.87, 1.48, 7.86	60.64 – 498.10	226.10	+++	heterogeneous	Cohesive Lumps

**Table 4 (continued) | Summary of the main characteristics observed by OM and colorimetry, according to the function of the mortars**

Samples	Function	Colours	L*, a*, b*	Size variation (µm)	Average size (µm)	Aggregate abundance	Distribution	Other observations
AG39c	U		60.54, 2.01, 7.24	69-08 – 1392.47	327.38	+++	heterogeneous	cracks. Ceramics, coal, lumps
AG40a	U		65.75, 10.65, 21.86	65.38 – 787.78	214.40	+++	heterogeneous	Pores, cracks Ceramics
AG41	U		60.95, 11.34, 19.62	41.49 – 679.72	211.32	++++	heterogeneous	Cracks Ceramics, coal

(S – structural, R – render, U – unclassified).

Aggregate abundance: high (++++), medium (+++), low (++)

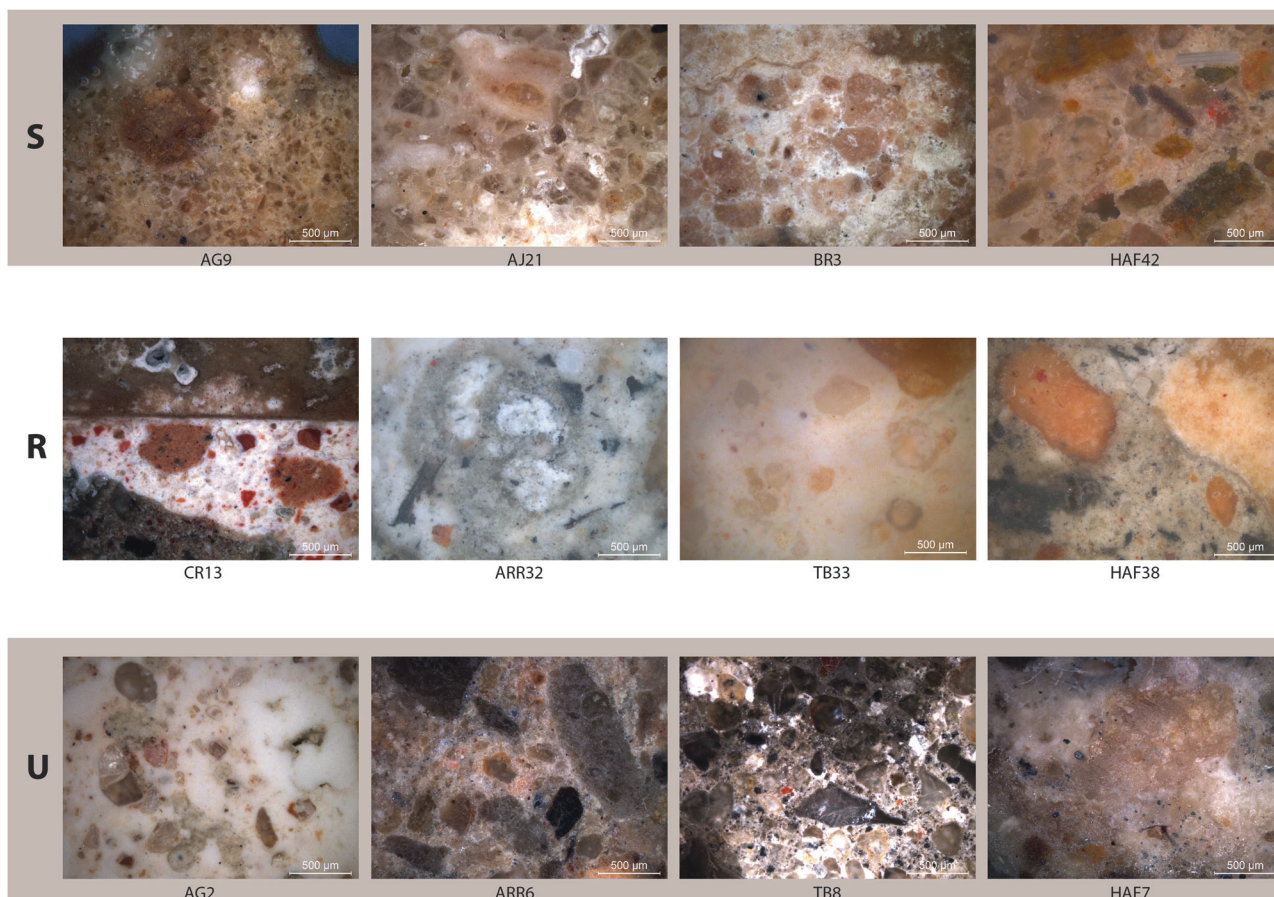


**Fig. 6 | Some of the mortar samples from the Carthage aqueduct, observed in cross-section, by OM. It is possible to perceive the variation in relation to the colours, size, shape, and distribution of the grains between the samples, including**

when considering the nomenclature established by the work team. (S – structural, R – render, U – unclassified).

materials used as coatings, the use of ceramic fragments and charcoal was observed more frequently. This result was also consistent with the function of the mortar, especially when considering its use as a coating of the water conduit, since this type of aggregate confers hydraulic properties to the material<sup>60</sup>. Regarding the identification of cement minerals, when identified, they corresponded to samples classified as modern materials, which confirms the indication made in situ.

Although it was not possible to identify a characteristic pattern in the samples according to the historical classification, it was possible to realise that, in this case, the general construction characteristics were more evident for this classification. However, it should be borne in mind that various factors will have an influence on the characteristics observed in the mortars and the way in which this material has come down to the present day, such as the origin of

the raw materials, work phases, production technology, application and the very history of use and reconstruction of the monument, which can make it difficult to directly relate the material to the historical period.

**Data availability**

All data generated or analysed during this study are included in this published article.

Received: 6 April 2025; Accepted: 29 October 2025;

Published online: 09 December 2025

**References**

1. Hoyos, D. *Carthage: A Biography* (Routledge, 2021).

2. Lancel, S., Picard, G.-C., Duval, N. & E.B. in 12 | *Capsa - Cheval* (ed. Publishers, P.) (Encyclopédie Berbère, 1993).
3. Saussure, H. De. L'aqueduc de Carthage. *Le Globe. Rev. genevoise géographie* **28**, 45–53 (1889).
4. Hodge, A. T. *Roman Aqueducts & Water Supply* (Duckworth, 2002).
5. Baklouti, H. Carthage et l'eau dans l'Antiquité. *Clim. Bioclimat la Tunisie, Tunis Univ. Tunis* **21–29** (2014).
6. Alvarez, A. et al. Characterisation of materials used in the Aqueduct of Zaghouan-Carthage (Tunisia) along construction and restoration periods. In *5th International Symposium Conservation of Monuments in the Mediterranean Basin* 5–8 (2000).
7. Figueiredo, M. O., Veiga, J. P. & Silva, T. P. Materials and reconstruction techniques at the Aqueduct of Carthage since the Roman period. *Hist. Constr. Guimarães Univ. do Minho* **391–400** (2001).
8. Ferchiou, N. Les aqueducs de Zaghouan à Carthage, et leurs structures complémentaires. Note préliminaire. *Africa* **17**, 69–86 (1999).
9. Figueiredo, M. O. et al. The construction of the Zaghouan-Carthage aqueduct (Tunisia). Structure, construction techniques and use of building materials. In *5th International Symposium on the Conservation of Monuments in the Mediterranean Basin* 378 (2000).
10. Leveau, P. Les aqueducs romains, le territoire et la 'gouvernance' de l'eau. In *Aquam-perducendam-curavit: captación, uso y administración del agua en las ciudades de la Bética y el occidente romano* (eds. Barrios, L. G. L., Palacios, J. L. C. & Pujol, L. P.) 1–20 (Universidad de Cádiz, 2011).
11. Rakob, F. A. Carthage l'aqueduc des thermes impériaux. *Les Dossiers l'Archéologie Dijon* **34–42** (1979).
12. Adam, J.-P. *Roman Building - Materials and Techniques* (Taylor & Francis Group, 2001).
13. Figueiredo, M. O., Veiga, J. P. & Silva, T. P. The Roman Aqueduct of Carthage: a minerochemical study on water conduit mortars and deposited crusts. In *9th International Congress on Deterioration and Conservation of Stone* (ed. Fassina, V.) 641–647 (Elsevier, 2002).
14. Frontinus. *The Stratagems and the Aqueducts of Rome* (W.H., 1925).
15. Dembskey, E. J. *The Aqueducts of Ancient Rome* (University of South Africa, 2009).
16. Nardo, D. *Roman Roads and Aqueducts* (ReferencePoint Press, 2015).
17. De Feo, G. et al. Historical and technical notes on aqueducts from prehistoric to medieval Times. *Water* **5**, 1996–2025 (2013).
18. Clamagirand, E., Rais, S., Chahcd, J., Gucfrj, R. & Smaoui, L. L' aqueduc de Carthage. *La Houille Blanche* **6**, 423–432 (1990).
19. Marta, R. *Architettura Romana: Técnica costruttive e forme architettoniche del mondo romano*. (Edizioni Kappa, 1990).
20. Arizzi, A. & Cultrone, G. Mortars and plasters—how to characterise hydraulic mortars. *Archaeol. Anthropol. Sci.* **13**, 144 (2021).
21. Corti, C. et al. Thermal analysis and archaeological chronology: the ancient mortars of the site of Baradello (Como, Italy). *Thermochim. Acta.* **572**, 71–84 (2013).
22. Leveau, P. Mortiers et bétons de tuileaux dans les aqueducs romains : le cas des aqueducs d'Arles et de Barbegal. *Mortiers Hydraul. en Méditerranée Antiq.* <https://doi.org/10.4000/books.pup.39945> (2021).
23. Vitruvio. *Tratado de Arquitectura* (IST Press, 2006).
24. Jackson, M. D. et al. Extreme durability in ancient Roman concretes. *Am. Ceram. Soc. Bull.* **97**, 22–28 (2018).
25. Arizzi, A. & Cultrone, G. Aerial lime-based mortars blended with a pozzolanic additive and different admixtures: a mineralogical, textural and physical-mechanical study. *Constr. Build. Mater.* **31**, 135–143 (2012).
26. Rispoli, C. et al. The ancient pozzolanic mortars of the Thermal complex of Baia (Campi Flegrei, Italy). *J. Cult. Herit.* **40**, 143–154 (2019).
27. Revuelta, M. B. *Construction Materials: Geology, Production and Applications* (Springer Nature, 2021).
28. Vitti, P. Mortars and masonry—structural lime and gypsum mortars in antiquity and middle ages. *Archaeol. Anthropol. Sci.* **13**, 164 (2021).
29. Artioli, G., Secco, M. & Addis, A. The vitruvian legacy: Mortars and binders before and after the Roman world. *Eur. Mineral. Union Notes Mineral.* **20**, 151–202 (2019).
30. Velosa, A. Luísa P. L. Argamassas de cal com pozolanas para revestimento de paredes antigas. (Universidade de Aveiro, 2006).
31. Caillat, P. Extrait d'une note sur la Restauration de l'Ancien Aqueduc de Carthage. *Rev. Archéologique* **26**, 292–301 (1873).
32. Briansó-Penalva, J. L. Study, characterization and analysis of degradation phenomena of ancient, traditional and improved building materials os geologic origin used in construction of historica monuments in the Mediterranean area. <https://www2.irb.hr/korisnici/obelici/euro-med/CA.htm> (2001).
33. Ergenç, D., Fort, R., Varas–Muriel, M. J. & Alvarez de Buergo, M. Mortars and plasters—how to characterize aerial mortars and plasters. *Archaeol. Anthropol. Sci.* **13**, 197 (2021).
34. Bouichou, M., Marie-Victoire, E., Texier, A. & Blondiaux, T. How to identify a natural cement: case study of the Vassy Church, France. In *3rd Historic Mortars Conference* 1–8 (2013).
35. Mohamed, A.-M. O., El Gamal, M. M. & Hameedi, S. M. in *Sustainable Utilization of Carbon Dioxide in Waste Management - Moving toward Reducing Environmental Impact* (Elsevier Inc., 2023).
36. Ramachandran, V. S., Paroli, R. M., Beaudoin, J. J. & Delgado, A. H. *Handbook of Thermal Analysis of Construction Materials* (Willian Andrew Publishing, 2003).
37. Aggelakopoulou, E., Bakolas, A. & Moropoulou, A. Lime putty versus hydrated lime powder: physicochemical and mechanical characteristics of lime based mortars. *Constr. Build. Mater.* **225**, 633–641 (2019).
38. Stoyanov, V., Kostova, B. & Dumanov, B. Analysis and characterization of modern and ancient mortars. *IOP Conf. Ser. Mater. Sci. Eng.* **1276**, 012001 (2023).
39. Moropoulou, A., Bakolas, A. & Bisbikou, K. Investigation of the technology of historic mortars. *J. Cult. Herit.* **1**, 45–58 (2000).
40. Moşoiu, C., Vlase, D., Vlase, G., Lazău, R. & Vlase, T. TG-DTA and FTIR analyses of roman and later historic mortars from Drobeta-Turnu Severin region. *J. Therm. Anal. Calorim.* **138**, 2159–2166 (2019).
41. Marques, S. F., Ribeiro, R. A., Silva, L. M., Ferreira, V. M. & Labrincha, J. A. Study of rehabilitation mortars: Construction of a knowledge correlation matrix. *Cem. Concr. Res.* **36**, 1894–1902 (2006).
42. Elsen, J., Balen, K. Van & Mertens, G. in *Historic Mortars - Characterisation, Assessment and Repair* (eds. Válek, J., Hughes, J. J. & Groot, C. J. W. P.) 125–139 (Springer, 2013).
43. Carvalho, F. et al. The case study of the medieval town walls of Gubbio in Italy: first results on the characterization of mortars and binders. *Heritage* **1**, 468–478 (2018).
44. Moropoulou, A., Bakolas, A. & Anagnostopoulou, S. Composite materials in ancient structures. *Cem. Concr. Compos.* **27**, 295–300 (2005).
45. Cantisani, E. et al. The binder of the 'Roman Concrete' of the Ponte di Augusto at Narni (Italy). *Period. di Mineral.* **71**, 113–123 (2002).
46. Casadio, F., Daher, C. & Bellot-Gurlet, L. Raman spectroscopy of cultural heritage materials: overview of applications and new fontiers in instrumentation, sampling modalities, and data processing. *Top. Curr. Chem.* **374**, 62 (2016).
47. Bersani, D. & Lottici, P. P. Raman spectroscopy of minerals and mineral pigments in archaeometry. *J. Raman Spectrosc.* **47**, 499–530 (2016).
48. Veiga, R. Air lime mortars: what else do we need to know to apply them in conservation and rehabilitation interventions? A review. *Constr. Build. Mater.* **157**, 132–140 (2017).
49. Arizzi, A. & Cultrone, G. The influence of aggregate texture, morphology and grading on the carbonation of non-hydraulic (aerial) limebased mortars. *Q. J. Eng. Geol. Hydrogeol.* **46**, 507–520 (2013).

50. Smith, D. C. A review of the non-destructive identification of diverse geomaterials in the cultural heritage using different configurations of Raman spectroscopy. *Geol. Soc. Spec. Publ.* **257**, 9–32 (2006).
51. de Faria, D. L. A. & Edwards, H. G. M. in *Raman Spectroscopy in Archaeology and Art History* (eds. Vandenberghe, P. & Edwards, H. G. M.) (The Royal Society of Chemistry, 2019).
52. Martínez-Ramírez, S. & Fernández-Carrasco, L. *Construction and Building: Design, Materials, and Techniques* (ed. Doyle, S. G.) (Nova Science Publishers, 2011).
53. Freeman, J. J., Wang, A., Kuebler, K. E., Jolliff, B. L. & Haskin, L. A. Characterization of natural feldspars by raman spectroscopy for future planetary exploration. *Can. Mineral.* **46**, 1477–1500 (2008).
54. Muralha, V. S. F., Rehren, T. & Clark, R. J. H. Characterization of an iron smelting slag from Zimbabwe by Raman microscopy and electron beam analysis. *J. Raman Spectrosc.* **42**, 2077–2084 (2011).
55. de Faria, D. L. A., Venâncio Silva, S. & de Oliveira, M. T. Raman microspectroscopy of some iron oxides and oxyhydroxides. *J. Raman Spectrosc.* **28**, 873–878 (1997).
56. Leslie, A. B. & Hughes, J. J. Binder microstructure in lime mortars: implications for the interpretation of analysis results. *J. Eng. Geol.* **257**, 263 (2002).
57. Rato, V. Influência da Microestrutura Morfológica no Comportamento de Argamassas. (Universidade Nova de Lisboa, 2006).
58. Santos, A. R. et al. Evolution of the microstructure of lime based mortars and influence on the mechanical behaviour: The role of the aggregates. *Constr. Build. Mater.* **187**, 907–922 (2018).
59. Stefanidou, M., Kesikidou, F. & Antoniadis, K. The role of application techniques for high performance traditional renders. *Procedia Environ. Sci.* **38**, 242–247 (2017).
60. Nogueira, R., Ferreira Pinto, A. P. & Gomes, A. Design and behavior of traditional lime-based plasters and renders. Review and critical appraisal of strengths and weaknesses. *Cem. Concr. Compos.* **89**, 192–204 (2018).

## Acknowledgements

The authors would like to thank Professor Philippe Leveau for the kind permission to use the image in Fig. 1a, originally published in the article 'Leveau, P. Les aqueducs romains, le territoire et la 'gouvernance' de l'eau. in *Aquam-perducendam-curavit: captación, uso y administración del agua en las ciudades de la Bética y el occidente romano* (eds. Barrios, L. G. L., Palacios, J. L. C. & Pujol, L. P.) 1–20 (Universidad de Cádiz, 2011), p.5. This study was supported by the FEDER funds through the COMPETE 2020 Programme and National Funds through FCT-Portuguese Foundation for

Science and Technology under the project ref. UIDB/50025/2020-2023 (Cenimat), UIDB/00729/2020, UIDP/00729/2020, LA/P/0140/2020 (Vicarte), GLAZE Project N°16375, 2023.16519.ICDT, LISBOA2030-FEDER-00753900 and SFRH/BD/145308/2019 (F. Carvalho).

## Author contributions

Conceptualisation, F.C.; methodology, F.C. and J.P.V.; validation, J.P.V., T.P.d.S. and M.M.R.A.L.; investigation, F.C., J.P.V., and T.P.d.S.; writing—original draft preparation, F.C.; prepared figures, F.C.; writing—review and editing, F.C., J.P.V., M.M.R.A.L. and T.P.d.S.; supervision, J.P.V. and M.M.R.A.L. All authors have read and agreed to the published version of the manuscript. All authors read and approved the final manuscript.

## Competing interests

The authors declare no competing interests.

## Additional information

**Correspondence** and requests for materials should be addressed to Fernanda Carvalho or João Pedro Veiga.

**Reprints and permissions information** is available at <http://www.nature.com/reprints>

**Publisher's note** Springer Nature remains neutral with regard to jurisdictional claims in published maps and institutional affiliations.

**Open Access** This article is licensed under a Creative Commons Attribution 4.0 International License, which permits use, sharing, adaptation, distribution and reproduction in any medium or format, as long as you give appropriate credit to the original author(s) and the source, provide a link to the Creative Commons licence, and indicate if changes were made. The images or other third party material in this article are included in the article's Creative Commons licence, unless indicated otherwise in a credit line to the material. If material is not included in the article's Creative Commons licence and your intended use is not permitted by statutory regulation or exceeds the permitted use, you will need to obtain permission directly from the copyright holder. To view a copy of this licence, visit <http://creativecommons.org/licenses/by/4.0/>.

© The Author(s) 2025